

Marine Wastewater Discharges from Multiport Diffusers. II: Unstratified Flowing Water

Xiaodong Tian, A.M.ASCE¹; Philip J. W. Roberts, F.ASCE²; and Gregory J. Daviero, A.M.ASCE³

Abstract: Laboratory experiments on the near-field mixing of buoyant plumes discharged from multiport diffusers into unstratified flowing water are reported. The spatial variation of dilution was measured by a newly developed three-dimensional laser-induced fluorescence system and a microconductivity probe. The near-field hydrodynamics are complex. The plumes discharged upstream dilute and merge more rapidly than those discharged downstream. Even with wide port spacing, the plumes eventually merge to form a laterally uniform surface wastefield. The density profile in this wastefield becomes gravitationally stable and suppresses mixing, marking the end of the near field. The value of the port spacing ratio, s/H , below which the discharge approximates a line plume is greater for discharge into a flowing current than into a stationary environment, so the port spacing plays a lesser role in a flowing current. The mixing and dilution that occurs in the surface layer is less than for a discharge into a stationary environment, and it decreases as the current speed increases. Semiempirical equations to predict the major near field characteristics are presented.

DOI: 10.1061/(ASCE)0733-9429(2004)130:12(1147)

CE Database subject headings: Ocean disposal; Outfall sewers; Wastewater disposal; Model studies; Dilution; Multi-port diffuser.

Introduction

To investigate the mixing of buoyant wastewater discharged from submerged ocean outfall diffusers, an extensive series of experiments has been performed for various discharge and receiving water conditions. The purpose of these experiments was to systematically measure the near-field characteristics of discharges from multiport diffusers over a range of port spacings from wide, resulting in individual plumes that do not merge, to narrow, resulting in plumes that quickly merge. The investigations focused on the case where the flows are driven mainly by source buoyancy and the effects of momentum are negligible, as this is the case most relevant to coastal sewage outfalls. As defined in the previous paper [Tian et al. (2004), hereafter referred to as Part I], the "near field" is the region that includes buoyant plume rise, surface interactions, transition to horizontal flow, and extends into some portion of the spreading layer. The end of the near field is where mixing generated by the discharge becomes insignificant. This is considered to be where near-field dilution no longer changes appreciably with distance, defined here as the location where dilution is within 10% of its ultimate value.

The experimental procedures and results in stationary unstrati-

fied water were presented in Part I. In the present paper, we report the experiments in flowing unstratified water. As in Part I, the diffuser consisted of T-shaped risers producing horizontally opposed buoyant jets. Tracer concentration fields and dilution were mapped by a three-dimensional laser-induced fluorescence (3DLIF) system supplemented by a precision microconductivity probe.

Analysis

The problem under consideration is sketched in Fig. 1. (The basic parameters are the water depth H , port diameter d , port or riser spacing s , total number of ports n , port exit velocity u_j , effluent density ρ_o , and ambient density ρ_a . The discharge can be characterized by the port spacing and by either point or line fluxes of volume, momentum, and buoyancy (see Table 1 in Part I). When the receiving water is flowing, two new variables are introduced. These are the current speed u , and the angle of the current relative to the diffuser, Θ . For these experiments, the diffuser was perpendicular to the current, i.e. $\Theta=90^\circ$. The dynamical effect of the current is expressed by a type of Froude number (Roberts 1979):

$$F = \frac{u^3}{b} \quad (1)$$

Where b =buoyancy flux per unit diffuser length. If $F \ll 1$, the flow is dominated by buoyancy; and if $F \gg 1$, the flow is dominated by the ambient current.

Different flow regimes can exist, depending on the value of F . Based on experiments with a slot source, Roberts (1979) found three possible flow regimes, Fig. 2. For weak current ($F < 0.2$), the flow has a normal plume-like pattern and forms a surface layer that spreads upstream (as a wedge) and downstream. As the current speed increases to $F > 0.2$ the plume cannot entrain all of the oncoming flow and maintains a free plume pattern. It becomes attached to the lower boundary and mixes over the depth; this is

¹Postdoctoral Researcher, School of Civil and Environmental Engineering, Georgia Institute of Technology, Atlanta, Georgia, 30332.

²Professor, School of Civil and Environmental Engineering, Georgia Institute of Technology, Atlanta, Georgia, 30332.

³Malcolm Pirnie, Inc., 104 Corporate Park Dr., White Plains, NY 10602-0751

Note. Discussion open until May 1, 2005. Separate discussions must be submitted for individual papers. To extend the closing date by one month, a written request must be filed with the ASCE Managing Editor. The manuscript for this paper was submitted for review and possible publication on September 10, 2003; approved on June 18, 2004. This paper is part of the *Journal of Hydraulic Engineering*, Vol. 130, No. 12, December 1, 2004. ©ASCE, ISSN 0733-9429/2004/12-1147-1155/\$18.00.

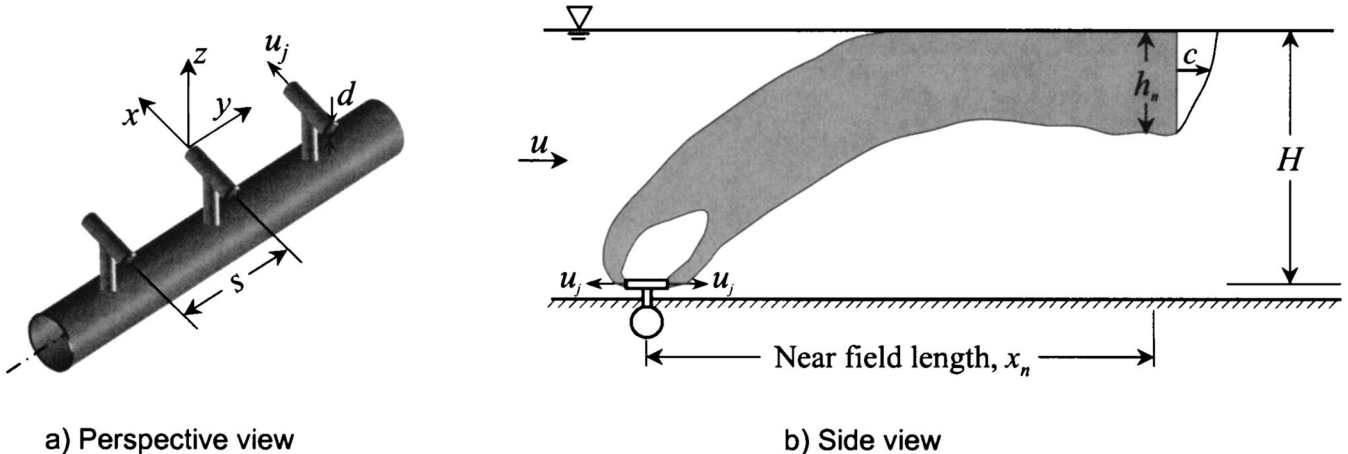


Fig. 1. Definition sketches

sometimes called the forced entrainment regime. Finally, when $F > 1$, the upstream wedge is expelled. The same flow regimes were reported by Davidson et al. (1993) from experiments with multiport discharges. In contrast, experiments with multiport diffusers reported by Mendez-Diaz and Jirka (1996) did not indicate mixing over depth even for Froude numbers up to $F = 8$. They attributed the fact that Roberts' (1979) experiments showed full mixing at lower Froude numbers to the slot source that did not allow ambient fluid to pass between the risers thereby satisfying the downstream entrainment. This observation is also supported by the experiments of Roberts et al. (1989) with a multiport diffuser (the same one used here). As can be seen in their Fig. 4, full mixing and bottom attachment was not observed for $F = 1$, but did occur as the current speed increased to $F = 10$ and beyond. The implication is that mixing over depth and bottom attachment for a multiport diffuser (at least one with risers with gaps in between) does not occur until the Froude number exceeds a critical value that lies somewhere between 1 and 10. This is discussed further in the results below.

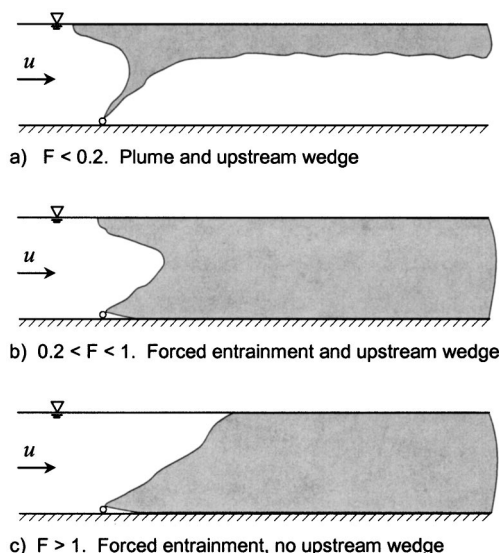


Fig. 2. Flow regimes for line plume in perpendicular current (after Roberts 1979)

Any dependent flow variable, ψ , can be expressed as

$$\psi = f(b, m, s, H, u) \quad (2)$$

with the usual assumptions: (1) That the flow is fully turbulent and therefore independent of the jet Reynolds number $R = u_j d / v$; (2) the Boussinesq approximation applies, i.e., variations in fluid density are small compared to absolute densities and so are dynamically only important as buoyancy forces; and (3) dynamic effects of the source volume flux are negligible. Furthermore, most outfalls operate such that the flow is driven mainly by the buoyancy flux so the effects of momentum flux, M , or m , can be neglected. As shown in Part I, these assumptions are usually satisfied for ocean outfall discharges. With the above assumptions, a dimensional analysis of Eq. (2) then yields:

$$\psi' = f\left(F, \frac{s}{H}\right) \quad (3)$$

where ψ' is a dimensionless form of the dependant variable. The wastefield characteristics of most interest here are (Fig. 1) the near-field dilution, S_n , the length of the near field, x_n , and the layer thickness, h_n . For these variables, Eq. (3) becomes (Daviero 1998):

$$\frac{S_n q}{u H} = f\left(F, \frac{s}{H}\right) \quad (4a)$$

$$\frac{x_n}{H} = f\left(F, \frac{s}{H}\right) \quad (4b)$$

$$\frac{h_n}{H} = f\left(F, \frac{s}{H}\right) \quad (4c)$$

Eq. (4) has two limiting cases that are of special interest; these are given below.

For $s/H \ll 1$, the ports are closely spaced so that the individual discharges quickly merge and behave like a line plume. The port spacing is then irrelevant, and Eq. (4) becomes:

$$\frac{S_n q}{u H} = f(F) \quad (5a)$$

$$\frac{x_n}{H} = f(F) \quad (5b)$$

$$\frac{h_n}{H} = f(\mathbf{F}) \quad (5c)$$

For $\mathbf{F} \ll 1$, the current has little effect and dilution can be predicted by the line plume equation for stationary receiving water [Eq. (9) of Part I], $S_n q / b^{1/3} H = 0.49$. This can be written in the notation of Eq. (5a) as

$$\frac{S_n q}{uH} = 0.49 \mathbf{F}^{1/3} \quad (6)$$

Eq. (6) applies for $s/H \ll 1$ and $\mathbf{F} \ll 1$. For a strong current (i.e., $\mathbf{F} \gg 1$), the discharge mixes over the depth [Fig. 2(c)], and Eq. (5a) becomes

$$\frac{S_n q}{uH} = C_1 \quad (7)$$

Eq. (7) applies for $s/H \ll 1$ and $\mathbf{F} \gg 1$. $C_1 = \text{constant}$ that Roberts (1979) estimated as being equal to 0.6 from experiments with a slot source. The value of C_1 determined from the presented experiments is given below.

For $s/H \gg 1$, the ports are widely spaced and the plumes do not merge. For weak currents (i.e., $\mathbf{F} \ll 1$), the point plume equations for stationary receiving water (Eqs. (10a) and (10b) of Part I) apply $S_n q / b^{1/3} H = 0.41(s/H)^{-2/3}$ or $S_n Q_j / B^{1/3} H^{5/3} = 0.26$. These can be written in the notation of Eq. (4a) as

$$\frac{S_n q}{uH} = 0.41 \mathbf{F}^{-1/3} \left(\frac{s}{H} \right)^{-2/3} \quad (8)$$

Eq. (8) applies for $s/H \gg 1$ and $\mathbf{F} \ll 1$. For a strong current (i.e., $\mathbf{F} \gg 1$), it would be expected that the plumes would be in (Wright 1977) the buoyancy-dominated far field [(BDFF) also referred to as an advected thermal]. The dilution relationship for this case is $SQ_j/uH^2 = C_2$, where C_2 is another experimental constant. This can be written in the notation of Eq. (4a) as

$$\frac{S_n q}{uH} = 2C_2 \left(\frac{s}{H} \right)^{-1} \quad (9)$$

Eq. (9) applies for $s/H \gg 1$ and $\mathbf{F} \gg 1$. From laboratory experiments, Chu (1979) estimated $C_2 = 0.41$ based on minimum dilution, and Wright (1977) estimated $C_2 = 0.25$ based on centerline dilution. Lee and Neville-Jones (1987) analyzed a data set compiled from in situ measurements of surface dilution in the sewage boil of several outfalls in the United Kingdom and some laboratory data and estimated $C_2 = 0.32$. Eq. (9) has often been proposed as being valid for ocean outfalls with widely spaced ports.

The applicability of these equations to the present results is evaluated below.

Experiments

The experiments were conducted in the test tank as described in Part I (see figure 1 in that paper). The towing system was used to simulate ambient currents. It consists of a carriage that rides on two precision 1 in. diameter rails running the length of the tank. The carriage is propelled via a chain and gear system by a 130 V Bodine motor connected in series to a Penta-Drive (KB Electronics, Coral Springs, Fla.) dc motor speed control device. The Penta-Drive provides the flexibility to vary the speed and direction of the towing carriage along the tank. The speed control was calibrated by timing the passage of the carriage between two points a known distance apart. The range of speeds is about 1 to

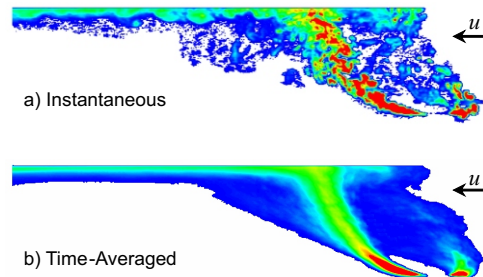


Fig. 3. Planar laser-induced fluorescence images of multiport diffuser in a crossflow $\mathbf{F}=1.6$, $s/H=4.5$

4 cm/s; faster speeds are not possible because tow durations are limited by the tank length. The charge coupled device camera is attached to the carriage and moves with it so that the discharge appears to be stationary relative to the camera in a flowing environment.

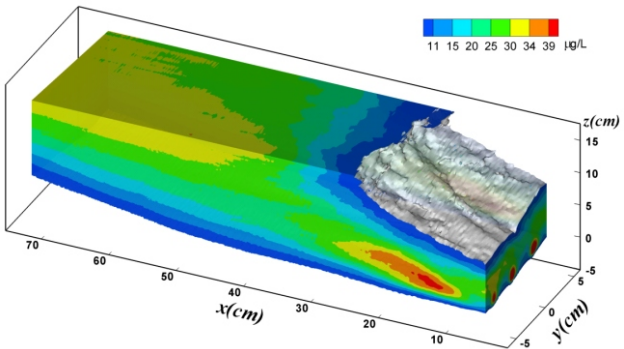
Dilutions were measured by the 3DLIF system and a microscale conductivity and temperature probe. The experimental systems and procedures were described in Part I, and the near-field length and layer thickness were determined as in that paper. 13 3DLIF and 43 conductivity probe experiments in flowing water were conducted. The number of risers was varied from 1 to 17. The parameter range investigated was $0.11 < s/H < 4.5$, $2.4 < H/l_M < 20.2$, and $2.1 < H/l_m < 30.5$. Most experiments were in the buoyancy-dominated region, [$H/l_M > 5$ and $H/l_m > 4$ (Brooks 1980)] as this is the case most relevant to ocean sewage outfalls. For summaries of the 3DLIF experiments, see Tian (2002), Table 5.3, and for the conductivity probe experiments, see Daviero (1998), Table 4.3.

Experimental Results

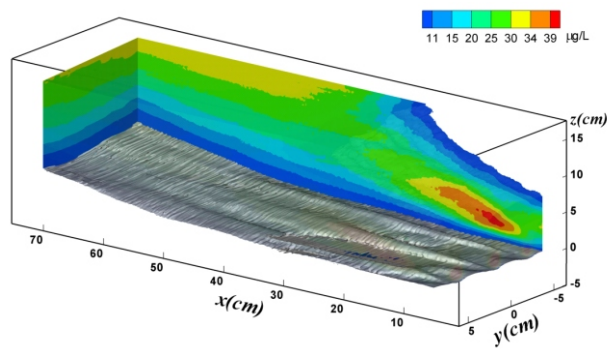
General Observations

The complexity of the plume dynamics in a flowing environment is evident from the instantaneous and time-averaged planar laser-induced fluorescence images shown in Fig. 3. The jets discharging upstream (counter-flowing jets) are quickly bent back by the current and experience rapid dilution. The jets discharging downstream (coflowing jets) are somewhat sheltered from the current so their deflection and rate of dilution is less than that of the upstream jets. Depending on the port spacing, the jets may first merge with their lateral neighbors and then with their upstream or downstream counterparts, or the upstream and downstream jets may first merge and then merge with their lateral neighbors. In all cases, however, lateral mixing and spreading will eventually result in a fully merged wastefield. This full merging may or may not occur within the near field. These processes are illustrated below for various conditions.

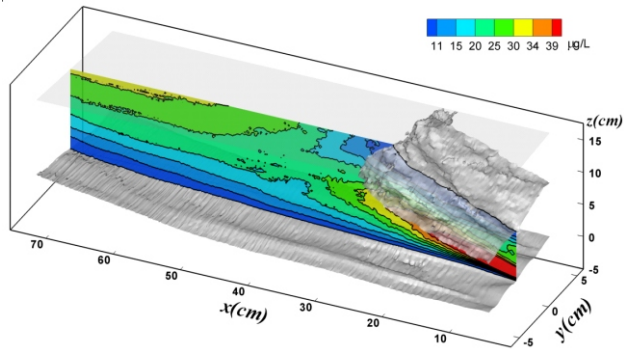
Figs. 4 and 5 show a discharge that approximates a line plume, $s/H=0.21$, with a Froude number, $\mathbf{F}=1.5$. Fig. 4 was generated by volume rendering of huge amounts of 3DLIF data (see Part I). The outer surface of the effluent field is shown as a gray isosurface, whose threshold concentration value is set just above zero. The magnitudes of local concentrations are displayed as pseudo-colors. Figs. 4(a and b) show top and bottom perspective views and Figs. 4(c and d) show top views with longitudinal and lateral concentration profiles made visible by making the outer isosur-



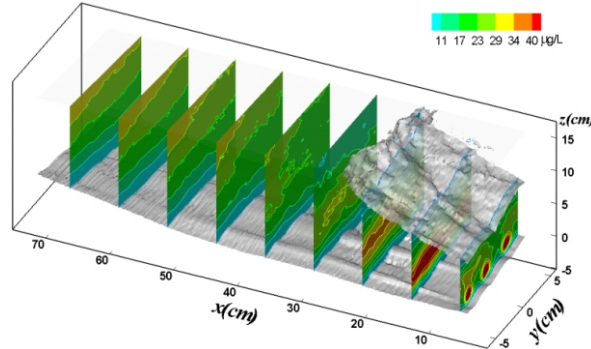
a) Top view



b) Bottom view



c) Longitudinal profile along centerline



d) Lateral profiles

Fig. 4. Three-dimensional laser-induced fluorescence visualizations for closely spaced ports ($F=1.5$, $s/H=0.21$, $c_o=1,500 \mu\text{g/L}$)

faces semitransparent. Only flows on the downstream side of the diffuser were captured, and, to include the end of the near field, the images begin just downstream from the diffuser. Only 3 of the 17 risers in this experiment are shown. Fig. 5 shows three-dimensional surface relief plots of lateral concentration profiles. In these plots, the height of the relief is the normalized tracer concentration, c/c_o .

The structure of the lateral profiles of Fig. 4(d) can be seen more clearly in the relief plots, Fig. 5. Close to the diffuser, at $x/H=0.3$, three upstream and three downstream jets are evident. The upstream jets (nearer the surface) are more dilute than the downstream jets and more merged due to their longer trajectory. The downstream jets are better defined with little merging and high centerline concentrations. By $x/H=0.6$, the pairs of horizon-

tally opposed jets have merged in the vertical, leaving three distinct structures in the horizontal. By $x/H=1.0$, the plumes have essentially become fully merged and show little lateral variability. This merged plume structure then continues to drift upward, mixing and diluting further as it rises. It eventually reaches the surface so that, at $x/H \approx 2.0$, surface concentrations have substantially increased. A stably stratified density profile then develops in the surface layer that suppresses vertical motions, until, at $x/H \approx 3.0$, mixing essentially ceases. This denotes the end of the near field, so in this case the plumes fully merge within the near field. The flow corresponds to that in Fig. 2(c): There is no upstream wedge, and the effluent extends over the water depth. Note, however, that this does not mean uniformly mixed over the depth, as can be seen from the profile at $x/H=3.0$.

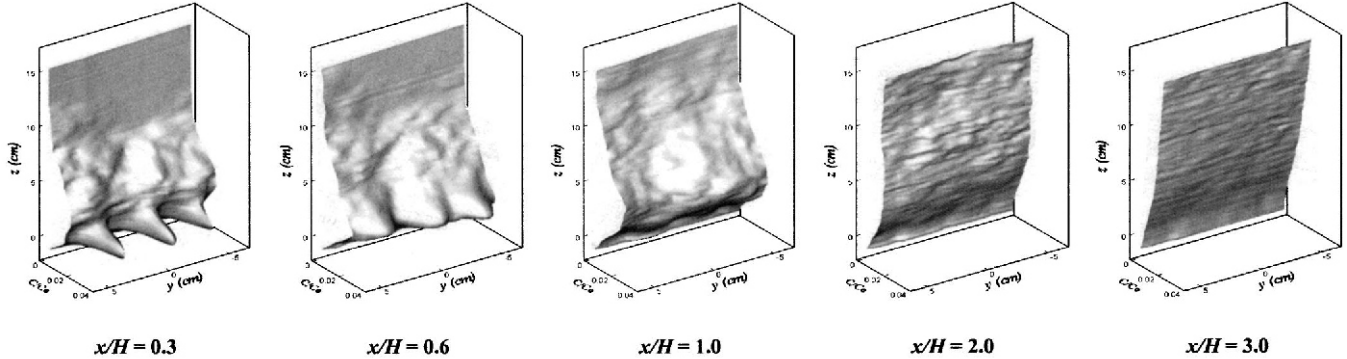


Fig. 5. Lateral concentration profiles for closely spaced ports ($F=1.5$, $s/H=0.21$)

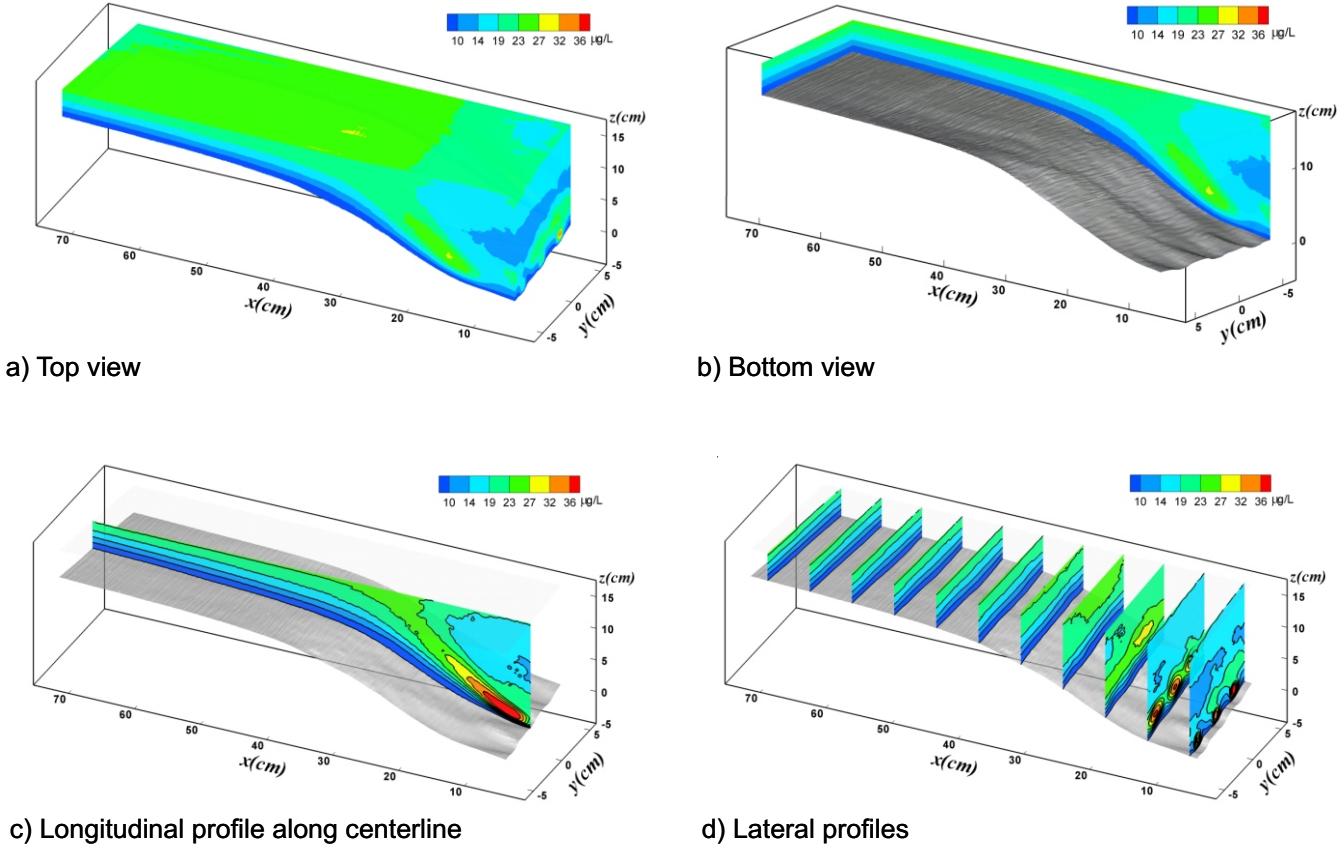


Fig. 6. Three-dimensional laser-induced fluorescence visualizations for closely spaced ports ($F=0.26$, $s/H=0.21$, $c_o=1,000 \mu\text{g/L}$)

Another case approximating a line plume ($s/H=0.21$) but with a smaller Froude number, $F=0.26$, is shown in Figs. 6 and 7. This flow is not mixed over the depth, as might be expected from Figs. 2(b). This supports the previous discussion that the transition Froude number at which forced entrainment occurs for multiport diffusers is greater than the value of 0.2 inferred from slot source experiments. An upstream wedge formed that is outside the field of view of Fig. 6. The longitudinal centerline profile, Fig. 6(c) does not indicate the layer thickening that is indicative of the presence of an internal hydraulic jump or rolling vortices (see Part I). These occur when the receiving water is stationary or the current is slow and disappear at higher current speeds. The value

of the critical Froude number where this occurs is undetermined, but Fig. 6 indicates that it is less than 0.26 for line plume conditions.

Lateral profiles are shown in Figures 6(d) and 7. At $x/H=0.5$, the upstream jets are fully merged and have reached the water surface while the downstream jets remain quite distinct. The downstream jets then drift upward, merging with their lateral neighbors and with their upstream counterparts. They are partially merged at $x/H=0.75$, and almost fully merged before reaching the water surface (see $x/H=1.0$). For $x/H \geq 1.5$, the plumes are fully merged and the concentration is laterally uniform. Again, a stable surface layer develops that suppresses turbulence and mix-

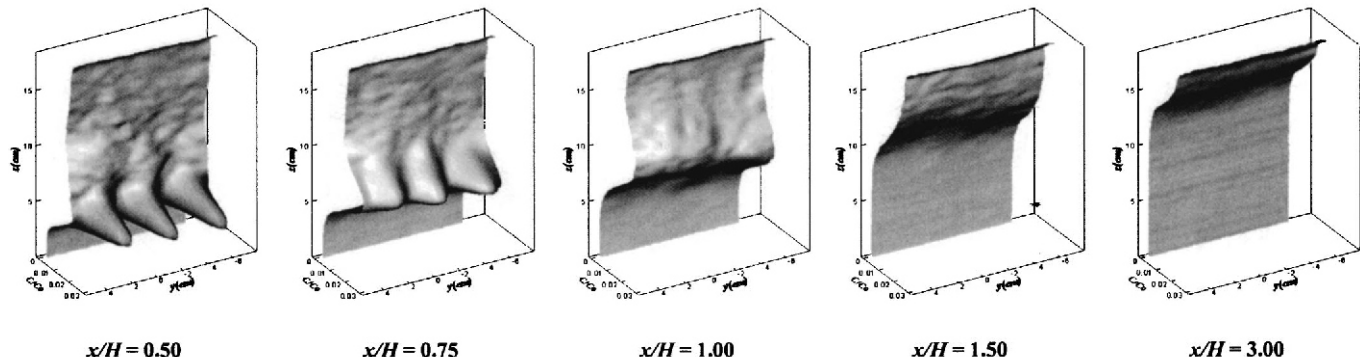


Fig. 7. Lateral concentration profiles for closely spaced ports ($F=0.26$, $s/H=0.21$)

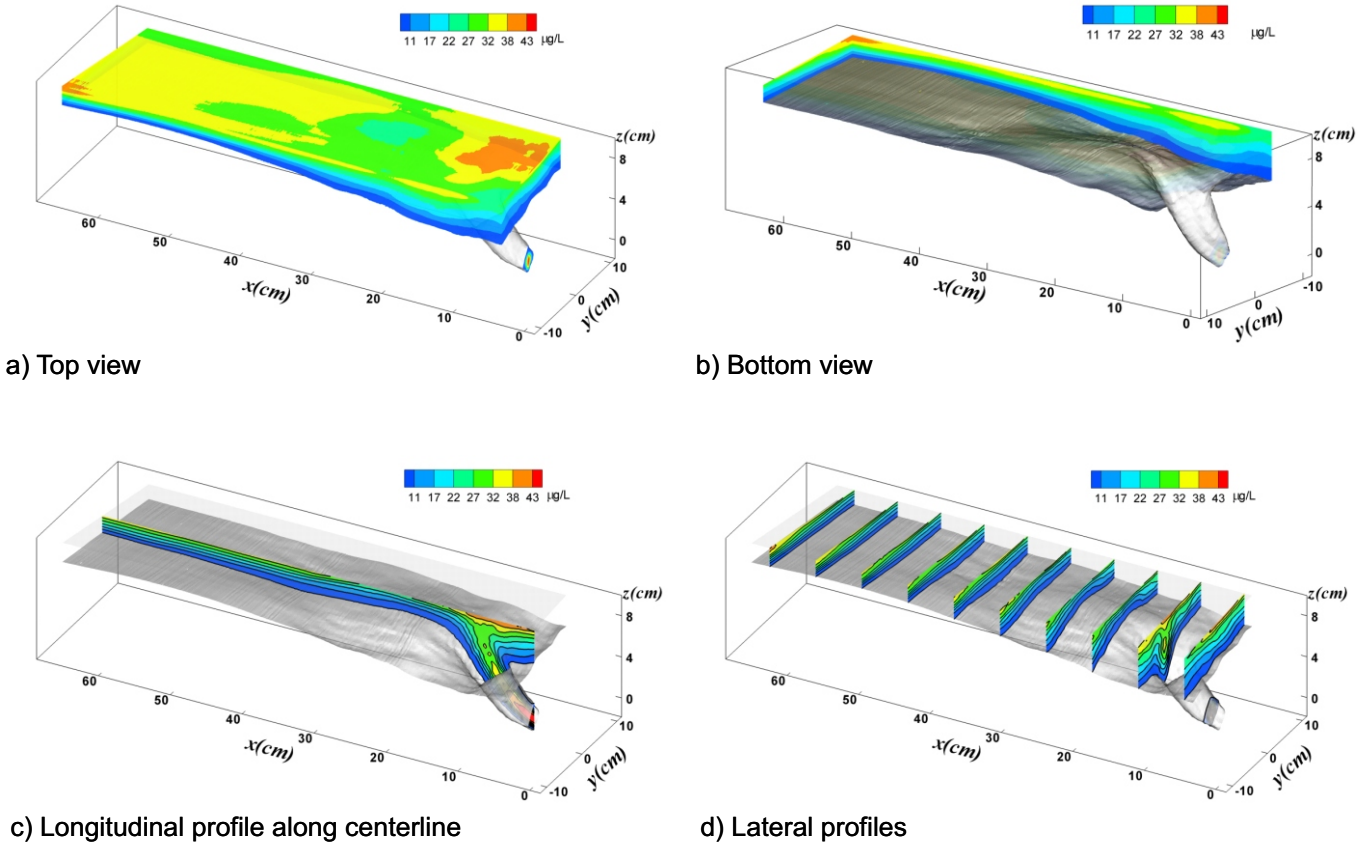


Fig. 8. Three-dimensional laser-induced fluorescence visualizations for widely spaced ports ($F=0.19$, $s/H=3.0$, $c_o=1,000 \mu\text{g}/\text{L}$)

ing. The length of the near field in this case is $x_n/H \approx 1.9$, so the plumes are again fully merged within the near field.

Finally, Figs. 8 and 9 show results for widely spaced ports, $s/H=3.0$, with $F=0.19$. Only one of the three risers in this experiment is shown. The surface layer is thin just downstream of the surface impaction point beyond which it thickens somewhat, suggesting an internal hydraulic jump or entrainment by rolling vortices (see Part I). The upstream jet is swept downstream. There is no merging for $x/H < 1.0$, but the lateral spreading and mixing that occurs beyond this point results in laterally uniform concentration by $x/H > 4.0$. Therefore, even with wide port spacing, the ultimate result is always the same: A laterally uniform field forms at some distance downstream with a stably stratified density field that suppresses further mixing. This defines the end of the near

field, with which these papers are mainly concerned. The length of the near field is $x_n/H \approx 3$ so the plumes do not become fully merged within the near field for this case.

Quantitative Results

Typical variations of dilution with downstream distance on the center line at the water surface for close and wide port spacings are shown in Fig. 10 [normalized according to Eq. (4a)]. For closely spaced ports ($s/H=0.21$), the surface impact point (the location of minimum surface dilution, see Figs. 6 and 7) occurs at $x/H \approx 1.3$. The dilution then increases monotonically towards its ultimate (near-field) value. This behavior is characteristic of flows

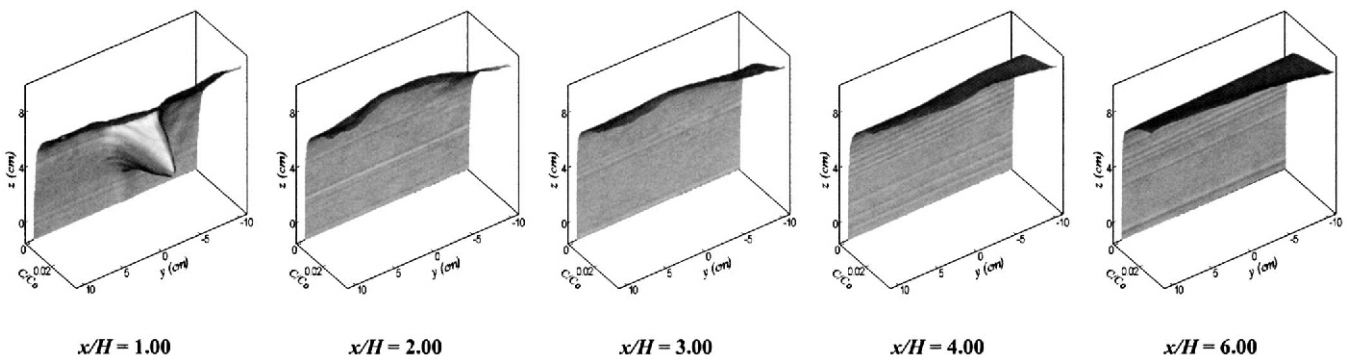


Fig. 9. Lateral concentration profiles for widely spaced ports ($F=0.19$, $s/H=3.0$)

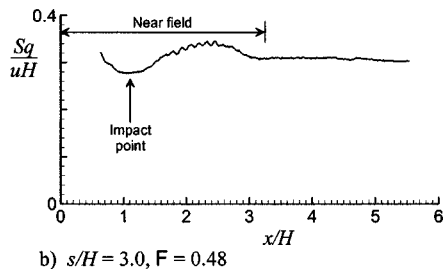
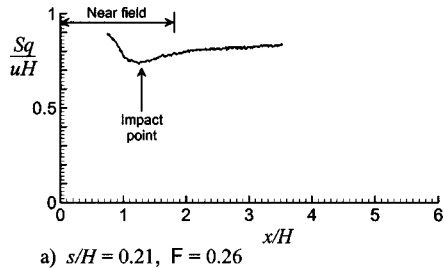
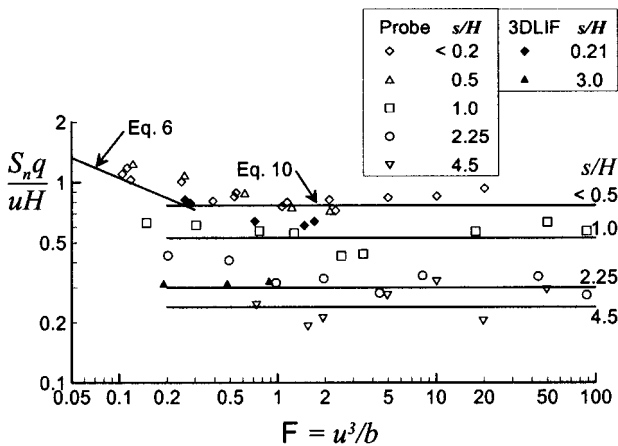
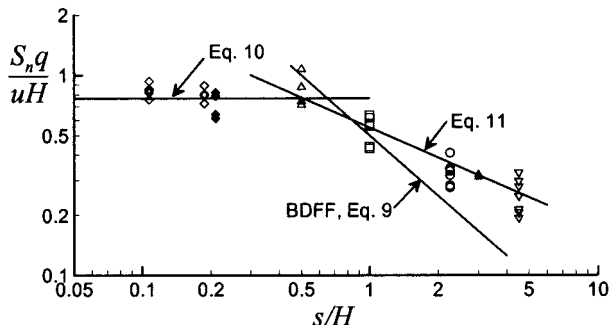


Fig. 10. Typical variations of surface dilution with downstream distance

with closely spaced ports in stagnant environments (Part I), except that the increase in dilution is less than the approximately 20% increase observed for that case. For widely spaced ports [Fig. 10(b)], the impact point is at $x/H \approx 1.4$. The dilution variation is again similar to stationary environments, whereby it increases to a maximum before finally decreasing toward its ultimate value.



a) As a function of Froude Number



b) As a function of port spacing for $F > 0.3$

Fig. 11. Near-field dilution

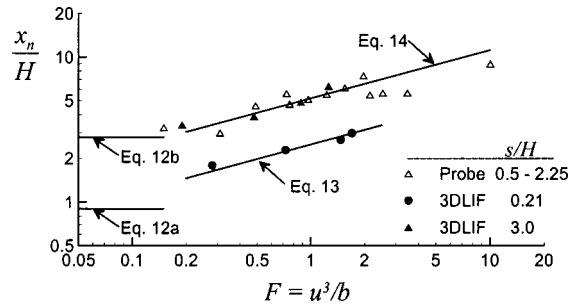


Fig. 12. Near-field length

mate value. The increase in dilution from the minimum to the near-field value is about 11%. This is also much less than the factor of about 3 increase for point plumes in stagnant environments reported in Part I.

The near-field dilutions for all experiments, normalized as in Eq. (4a) are plotted as a function of Froude number in Fig. 11(a).

For closely spaced ports, there should be no effect of spacing and the flow should behave like a line plume [Eqs. (6) and (7)]. Fig. 11(a) suggests that this occurs for $s/H \leq 0.5$. For $F < 0.1$, the results approximate the equation for unstratified stationary environments, Eq. (6); in other words, the current does not affect dilution when $F < 0.1$. This was also observed for slot plumes in unstratified currents by Roberts (1979) and for multiport diffusers in stratified currents by Roberts et al. (1989). As the current speed increases beyond $F = 0.1$, the dilution increases. For $F > 0.3$, the effluent mixes over the depth and the normalized near-field dilution becomes constant [Eq. (7)]. A best fit to the data yields $C_1 \approx 0.77$, so

$$\frac{S_n q}{uH} = 0.77 \pm 15\% \quad (10)$$

Eq. (10) applies for $s/H < 0.5$ and $F > 0.3$. If the effluent were uniformly mixed over depth, C_1 would be equal to one. It is less than this because the stable density profile that develops in the surface layer prevents uniform mixing over the water depth in the near field (Roberts 1979). The value of C_1 obtained here is larger than $C_1 = 0.6$ suggested by Roberts (1979) but should be more applicable to real diffusers, as Roberts' (1979) experiments were conducted with a slot source.

For wider ports spacings, the normalized dilution $S_n q / uH$ also becomes independent of F and is constant for $F > 0.3$ (albeit with considerable scatter). This is shown in Fig. 11(b) where the results for $F > 0.3$ are plotted versus port spacing, s/H . As the spacing increases, it might be expected that the results would eventually tend to those for individual isolated plumes in BDFF [Eq. (9)]. It can be seen, however, that this equation (with $C_2 = 0.25$) does not describe the results. An empirical equation that fits the data better in the range $0.5 < s/H < 4.5$ is

$$\frac{S_n q}{uH} = 0.55 \left(\frac{s}{H} \right)^{-1/2} \pm 20\% \quad (11)$$

[Daviero (1998) suggested $S_n q / uH = 0.60(s/H)^{-2/3}$ but Eq. (11) gives a better fit to the data.] In the other words, the results still show a dependence on port spacing even when the spacing is quite large. This is because of spreading and merging in the surface layer as discussed above. It indicates that point-plume results may not be widely applicable for prediction of near-field dilution of multiport diffusers in flowing currents.

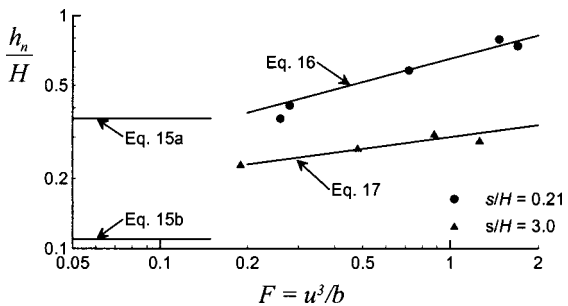


Fig. 13. Spreading layer thickness

The variation of near-field length, x_n , with Froude number is shown in Fig. 12. Also shown are the equations for the stagnant conditions from Part I:

$$\frac{x_n}{H} = 0.90 \quad (\text{for a line plume}) \quad (12a)$$

$$\frac{x_n}{H} = 2.80 \quad (\text{for a point plume}) \quad (12b)$$

The near-field length increases with increasing current speed. For $s/H=0.21$, i.e., a line plume, the results are approximated by

$$\frac{x_n}{H} = 2.5F^{1/3} \pm 20\% \quad (13)$$

For wider port spacings (in the range $0.5 \leq s/H < 4.5$), the near-field length shows no systematic dependency on spacing and a fit to the data is

$$\frac{x_n}{H} = 5.2F^{1/3} \pm 10\% \quad (14)$$

The near-field length is therefore directly proportional to the current speed for both cases.

As for the stagnant case, increasing s/H above the line plume limit increases the near-field length. This is mainly due to the internal jump or vortices that can be prominent for point plumes. They are not evident for line plume conditions (e.g. Figs. 4 and 6), and the surface dilution increases monotonically from its minimum value to the ultimate (near-field) value. The end of the near field is near the plume impact point. For wider spacing (e.g. Fig. 8), vortices may occur and the surface dilution passes through a maximum before decreasing to its ultimate value. This moves the end of the near field farther from the surface impact point. These effects are more prominent at low Froude numbers, and it is possible that the lengths of the near fields for point and line plumes approach each other for Froude numbers higher than could be measured here.

The variations of spreading layer thickness, h_n , with Froude number for $s/H=0.21$ and 3.0 are shown in Fig. 13. Again, the stagnant equations from Part I are shown:

$$\frac{h_n}{H} = 0.36 \quad (\text{for a line plume}) \quad (15a)$$

$$\frac{h_n}{H} = 0.11 \quad (\text{for a point plume}) \quad (15b)$$

Fits to the data with flowing currents are

$$\frac{h_n}{H} = 0.65F^{1/3} \pm 15\% \quad (\text{for } s/H = 0.21) \quad (16)$$

$$\frac{h_n}{H} = 0.3F^{1/6} \pm 10\% \quad (\text{for } s/H = 3.0) \quad (17)$$

The thickness increases with increasing Froude number in both cases. The normalized thickness h_n/H does not become unity (i.e., mixed over the depth) because of the thickness definition used here: The lower layer boundary is where the tracer concentration is 10% of the maximum (surface) value. No thickness data are available for other port spacings.

Discussion

The line plume equations for near field dilution [Eqs. (6) and (7)] apply for $s/H \leq 0.5$. Increasing the port spacing beyond this value caused the results to deviate from the line plume result, but they never became independent of port spacing, at least up to $s/H = 4.5$. Although Wright's (1977) BDFF result for an isolated port [Eq. (9)] might be expected to apply in this range, it did not. The flow is still in a transition where the ports are neither close enough to approximate a line source nor wide enough to be independent of each other. Dilution in this range ($0.5 < s/H < 4.5$) can be estimated by the empirical Eq. (11). Experiments for $s/H > 4.5$ could not be performed because of the limited tank size, so the spacing s/H at which near-field dilution becomes independent of port spacing could not be determined.

The increase in dilution beyond the surface impact point is smaller than those reported for stationary environments in Part I, and the increase becomes less significant as the current speed increases. This is because the large-scale rolling vortices that are the main mechanism of additional mixing in the horizontal spreading layer (see Discussion, Part I) were only observed at low current speeds. Above some critical current speed, or Froude number, these vortices disappear and no longer contribute to mixing. The value of the Froude number where this occurs is unknown, but vortices were not observed for line plume conditions for $F \geq 0.26$ and for wide port spacing for $F \geq 0.7$. For these cases, the surfaces impaction point essentially marks the end of the near field.

The presence of a flowing current increases the upper limit of the port spacing ratio s/H where the discharge approximates a line plume. This is because the longer plume trajectories afforded increased opportunity for merging. For closely spaced ports, the individual plumes merge completely before reaching the water surface (Figs. 4–7, whereas in a stationary environment they are only partially merged (Figs. 3 and 4 in Part I). According to part I, the discharge behaves like a line plume in stationary water for $s/H < 0.3$. In a flowing environment, it behaves like a line plume for $s/H < 0.5$, even for Froude numbers as low as 0.2. As discussed in Part I, the value of $s/H = 0.3$ is wider than often considered to be the limit above which port spacing affects mixing. The present results show that, in flowing water, the effects of port spacing are even less, so line plume results should have wide applicability to ocean sewage outfalls.

Conclusions

Experimental results on the near-field mixing of buoyant plumes discharged from multiport diffusers over a range of port spacing

into unstratified flowing water are presented. The flows are quite complex, with the jets discharged upstream undergoing more rapid dilution and merging than those discharged downstream. Depending on current speed, the jets may merge with their lateral neighbors before the upstream and downstream jets merge. With closely spaced ports, the plumes merge before impacting the water surface; for widely spaced ports, they do not. In all cases, even with very wide port spacing, the plumes will eventually merge to form a laterally uniform surface wastefield. This merging may or may not occur within the near field. The end of the near field is marked by suppression of further mixing by the stably stratified density profile that develops in the surface wastefield.

The discharge behaves like a line plume for $s/H \leq 0.5$. This upper limit of port spacing is greater than the value of 0.3 reported for discharges into a stationary environment in part I because of the presence of the current. The discharge is in transition from a line to a point plume at least up to $s/H = 4.5$.

Some additional mixing (and dilution) occurs beyond the point where the plume impacts the water surface. The additional dilution is much less than when the discharge is into a stationary environment, and decreases as the current speed increases. Above some current speed (or Froude number), the additional mixing is negligible. The value of the Froude number beyond which additional mixing becomes negligible was not investigated, but it appears to be less than 0.26 for line plume conditions.

Because of merging and mixing in the surface layer, equations for isolated plumes that have been previously proposed by others do not appear to be applicable, at least for the range of port spacings investigated which includes widely spaced port up to $s/H = 4.5$. Alternative empirical and semiempirical equations to predict near-field characteristics are presented.

Acknowledgements

The writers acknowledge the support of the National Science Foundation under Grant Nos. DGE-9354986 and CBT-8915537 and the STAR program of the U. S. Environmental Protection Agency, Exploratory Research, Physics, Grant Number R826216. Ms. Karen Maile is also thanked for her help in conducting the conductivity probe experiments.

Notation

The following symbols are used in this paper:

- b = line-source buoyancy flux;
- C_1 = experimental constants;
- c = local tracer concentration;
- c_o = source tracer concentration in the outfall pipe;
- d = port diameter;

- F = Froude number;
- g = acceleration due to gravity;
- H = water depth;
- h_n = thickness of wastefield at end of near field;
- l_M = point-source length scale;
- l_m = line-source length scale;
- m = line-source momentum flux;
- n = total number of ports;
- Q_j = flowrate per port;
- Q_T = total flow rate from diffuser;
- q = flowrate per unit diffuser length;
- R = jet Reynolds number;
- S = dilution;
- S_n = near field dilution;
- s = port spacing;
- u = current speed;
- u_j = port exit velocity;
- x_n = length of near field;
- ρ_a = ambient density at level of ports;
- ρ_o = effluent density;
- ν = kinematic viscosity; and
- ψ, ψ' = arbitrary variables.

References

- Brooks, N. H. (1980). "Synthesis of stratified slow phenomena for design of outfalls." *Proc., 2nd Int. Sec. Int. Symp. on Stratified Flows*, 809–831.
- Chu, V. H. (1979). "L.N. Fan's data on buoyant jets in crossflow." *J. Hydraul. Div., Am. Soc. Civ. Eng.*, 105(5), 612–617.
- Daviero, G. (1998). "Hydrodynamics of ocean outfall discharges in unstratified and stratified flows." PhD Thesis, School of Civil Engineering, Georgia Institute of Technology, Atlanta.
- Davidson, M. J., Papps, D. A., and Wood, I. R. (1990). "The behavior of merging buoyant jets." *Recent research advances in the fluid mechanics of turbulent jets and plumes*, Viana do Castelo, Portugal, June.
- Lee, J. H. W., and Neville-Jones, P. (1987). "Initial dilution of horizontal jet in crossflow." *J. Hydraul. Eng.*, 113(5), 615–629.
- Mendez-Diaz, M. M., and Jirka, G. H. (1996). "Buoyant plumes from multiport diffusers in deep coflowing water." *J. Hydraul. Eng.*, 122(8), 428–435.
- Roberts, P. J. W. (1979). "Line plume and ocean outfall dispersion." *J. Hydraul. Div., Am. Soc. Civ. Eng.*, 105(4), 313–330.
- Roberts, P. J. W., Snyder, W. H., and Baumgartner, D. J. (1989). "Ocean outfalls I. Submerged waste fields formation." *J. Hydraul. Eng.*, 115(1), 1–25.
- Tian, X. (2002). "3DLIF and its applications to studies of the near-field mixing of wastewater discharges." PhD thesis, School of Civil and Environmental Engineering, Georgia Institute of Technology, Atlanta.
- Tian, X., Roberts, P. J. W., and Daviero, G. J. (2004). "Marine wastewater discharges from multiport diffusers. I: Unstratified stationary water." *J. Hydraul. Eng.*, 130(12), 1137–1146.
- Wright, S. J. (1977). "Mean behavior of buoyant jets in a crossflow." *J. Hydraul. Div., Am. Soc. Civ. Eng.*, 103(5), 499–513.